

# Weathering variations in a granitic massif and related geotechnical properties through seismic and electrical resistivity methods

Javier Olona\*, Javier A. Pulgar, Gabriela Fernández-Viejo, Carlos López-Fernández and Juan M. González-Cortina

Department of Geology, University of Oviedo, Jesus Arias de Velasco s/n, 33005 Oviedo (Asturias), Spain

Received December 2009, revision accepted July 2010

## ABSTRACT

Mapping and distribution with depth of alteration in rocks is critical in engineering planning because it has a fundamental impact on the geotechnical properties of the materials. Lateral heterogeneity on a weathered rock massif makes boreholes inadequate for its complete characterization. Geophysical methods increase spatial sampling along the study area and can be related to geotechnical parameters, so subsoil conditions can be better understood.

In order to determine its geotechnical qualities and variability along two different profiles, we attempt to characterize a granite massif in north-west Spain by the integration of results from seismic refraction, multichannel analysis of surface waves (MASW) and electrical resistivity tomography methods (ERT). The study area, the so-called Carlés granite, shows all the weathering grades from sandy soil to fresh rock. A reference borehole where samples were taken and laboratory measurements were made, serves as a direct check for the results of one of the profiles, the other being interpreted without any direct information. This approach has permitted the evaluation of the advantages and limitations of each geophysical method and created an accurate geotechnical model of the massif, correlating physical and geotechnical parameters such as rock quality designation, weathering grade, or standard penetration test.

The field seismic velocities have been compared with the ultrasonic measurements at the laboratory, permitting an evaluation of the field and laboratory elastic constants. The trend in the values of these parameters agrees with the field and laboratory test for the shallow parts of the massif. However, unrealistic elastic constants have been obtained for fresh rock based on the results of the field experiments. This is related to an apparent underestimation of the velocity of seismic S-waves for the deepest layers. This fact suggests that the methodology followed throughout this work is able to provide a full geotechnical model of an altered rock massif for the first tens of metres, discriminating between different weathered levels. It is also useful and reliable when inferring elastic constants for depths of up to 20 m. However, its validity becomes doubtful with depth, so care must be taken when calculating elastic moduli and trying to extrapolate directly to a rock massif.

## INTRODUCTION

The weathering and alteration of granite massifs has a fundamental impact on their geotechnical or hydrogeological properties (Begonha and Braga 2002; Lan *et al.* 2003; Dewandel *et al.* 2006). Weathering processes involve the biogeochemical hydrolysis of the rock's mineral constituents and their mineral transformations under new surface conditions (Tardy 1971). These processes give place to a completely different working ground

distribution from a geotechnical point of view, making a study of the alteration of granite massifs compulsory when planning and performing any engineering project through them. At the same time, weathered granite as a raw material for construction purposes has its own economic importance.

An accurate geotechnical site characterization inside a weathered massif is a difficult task, due to the irregular distribution of any alterations and the lateral and vertical variation of rock properties, which means that the use of single boreholes is a relatively costly method, when trying to study the full granitic massif.

\* olona@geol.uniovi.es

Benson *et al.* (2003) showed that borehole densities are commonly inadequate to detect geological anomalies. Geophysical methods improve the probability of detecting and delineating subsoil features with continuous measurements and can be used to reduce the budget and time invested in a geotechnical study. Geophysical methods may also be used as a tool for preliminary site investigation in order to identify areas that should later be earmarked for drilling.

The objective of our study was to determine the variability of the geotechnical properties of the Carlés granite massif, which showed various levels of weathering, from fresh rock to altered rock that has been converted into loose sandy soil. The geophysical methods selected for the study were seismic refraction, multichannel analysis of surface waves (MASW) and electric resistivity tomography (ERT). The seismic refraction method has been traditionally used for the detection of the upper bedrock or basement interfaces, the measurement of weathering layer thicknesses, or the evaluation of fracturing (Lee and Freitas 1990). MASW is a relatively new method with ample potential for engineering related surveys. It allows the stiffness of the subsoil and the intrinsic parameters of geological materials to be evaluated for the characterization of the geotechnical quality of the subsoil. MASW has been employed successfully for studying faults and related weathering zones (Ivanov *et al.* 2006), or to map bedrock (Miller *et al.* 1999). ERT, as well as seismic refraction, is a widely used geophysical method for geotechnical application due to its ease for use and reliability. The method has been applied to geotechnical studies that involve mapping shallow geology, faults (Fazzito *et al.* 2009) and/or for correlation between geotechnical parameters (Friedel *et al.* 2006).

The second part of our study consisted of a series of laboratory tests measuring the density, open porosity and ultrasonic P ( $V_p$ ) and S ( $V_s$ ) seismic wave velocities of core samples taken from the borehole drilled in the granite along one of the profiles

selected. The main goal of the laboratory test was the comparison of the elastic constants calculated from the field seismic velocities with the constants calculated from the ultrasonic velocities.

The final integration of all of the data has permitted a more accurate geotechnical characterization of the study area and a baseline to continue the geophysical interpretation of other parts of the massif where boreholes are not being made.

This work is part of a more extended and in-depth PhD thesis study of geophysical characterization in different geological settings, including not only altered granite but also alluvial grounds or fractured quartzite. The final objective is to apply this multi-technique methodology to different geotechnical settings in order to be able to produce zone conclusions in related fields, such as hydrogeological or geological studies. In addition, we hope to improve the resolution of field interpretations by taking into account the advantages and shortcomings of each method.

## GEOLOGICAL SETTING

The Carlés granite massif is situated in the so-called Cantabrian zone of the Variscan Massif in north-west Spain (Lotze 1945; Julivert *et al.* 1972), between the town of Carlés and the Narcea River, 50 km west of Oviedo city (Fig. 1). This Carboniferous granite is a small (0.5 km<sup>2</sup>) calc-alkaline monzogranite (Solé *et al.* 1995), intruded into the upper siliciclastic Furada Formation (late Silurian) and the carbonatic Rañeces Group (early Devonian), which presents all kinds of grades of weathering, from loose sandy soil to fresh rock. A geophysical survey was planned including two study lines along which 2D seismic refraction data, MASW and ERT data (Fig. 1) were acquired. In Line 1, the geophysical data were compared with direct samples from a borehole.

The borehole was drilled up to 35.7 m depth in the granite. Based on the International Society for Rock Mechanics (Brown 1981) weathering grade classification (Table 1), the Carlés granite

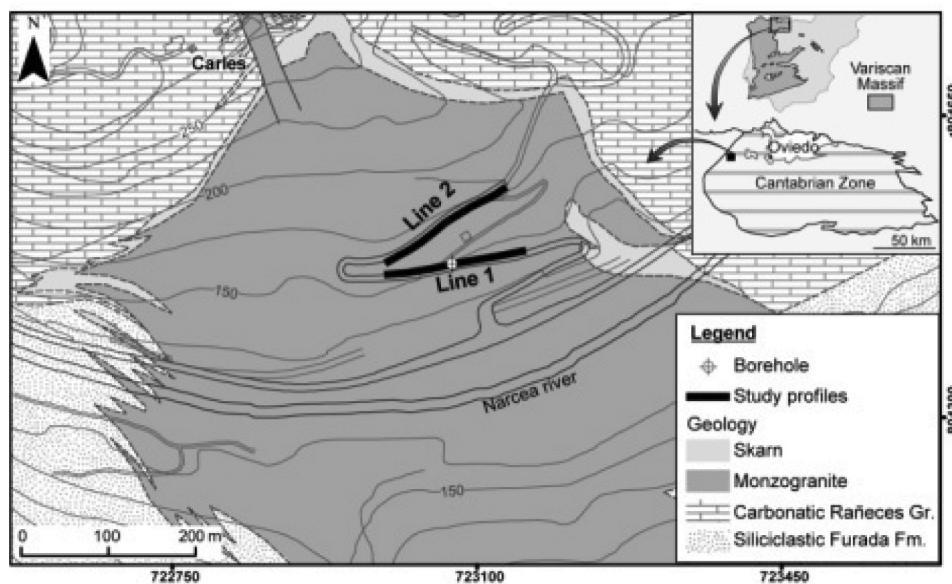


FIGURE 1 Geological map of the Carlés granite (geology after Martin-Izard *et al.* 2000). In thick black lines the two geophysical study profiles (Line 1 and Line 2) and the borehole, located at the centre of Line 1.

TABLE 1  
Weathering classification by Brown (1981)

Class	Term	Description
I	Fresh rock	No visible sign of rock material weathering
II	Slightly weathered rock	Discoloration indicates weathering of rock materials and discontinuity surfaces
III	Moderately weathered rock	Less than half of the rock material is decomposed and/or disintegrated to soil
IV	Highly weathered rock	More than half of the rock material is decomposed and/or disintegrated to soil
V	Completely weathered rock	All rock material is decomposed and/or disintegrated to soil. The original mass structure is still largely intact
VI	Residual soil	All rock material is converted to soil. The mass structure and material fabric are destroyed

samples show a first level of rock highly-weathered into sandy soil (class V–VI, classified as SM by the Unified Soil Classification System) between 0–11.4 m depth (Fig. 2). A granulometric analysis shows that the soil is composed mainly of sands (with 92% of particles between 2–0.06 mm), together with 8% of smaller silt-clay particles. To evaluate the state of the soil *in situ*, a standard penetration test (SPT) was made. *SPT-N* values suggested stiff soil for depths of 2.5 m changing to very dense soil at 5 m until 11.4 m, where the test was not applicable. A second level, from 11.4–19.5 m, shows weathered granite (class III) with alteration colours and thin levels of fresh granite. From 19.5 m to the end of borehole at 35.7 m, the granite responds to class I–II (poorly or null weathered). The low rock quality designation of 17% from 11.4 m until 19.5 m is the result of the high degree of alteration. Below 19.5 m, rock quality designation gradients of 54–57% depend on the fracturation of the massif, which diminishes with depth, reaching 95% at the end of borehole. There is a low rock quality designation level between 33–34.4 m, which corresponds to a subvertical quartz vein destroyed during the drilling process. Fracture surfaces are generally flat and clean or with a slight infill of white clay. Water did not appear in the borehole at all.

## METHODOLOGY

The methodology followed in this study both in the field and in the laboratory is described below, starting with the field data (acquisition parameters for each experiment and the modelling procedures) and then detailing the laboratory measurements and sampling.

## FIELD GEOPHYSICAL METHODS

### Seismic refraction

Seismic refraction is based on the analysis and interpretation of the first arrivals of critically refracted waves in order to provide a two-dimensional seismic P-wave velocity model. Seismic velocities of rocks and soils depend on a variety of parameters such as density, porosity, saturation grade and the characteristics of the saturation fluid, the weathering state, effective stress and the level of fracturation (fracture density, length, aperture, infilling material and the areal fraction of surfaces in contact). Because in near-surface geophysics an increment in P-wave velocity implies a better material from a geotechnical point of

view (i.e., an increment in  $V_p$  could be related to a decrease in the weathering grade or the fracturation density inside a rock massif), the  $V_p$  model allows the evaluation of the subsoil along a survey line. However, we need to keep in mind that  $V_p$  is sensitive to changes in saturation grade, too.

Acquisition was performed with a Geometrics Stratavisor NX and 60 geophones of 4.5 Hz spaced 2 m apart. The seismic source was a 5 kg sledgehammer strike on an aluminium plate on the ground. Strikes were spaced 10 m apart from the beginning to the end of the spread, with a total of 13 shots. Figure 3 shows the typical record sections obtained for each line.

Modelling was performed with tomographic software based on a Monte Carlo-based optimization scheme called generalized simulated annealing (Bohachevsky *et al.* 1986), which inverted first-arrival times for velocities without prior assumptions of the subsurface velocities as input (Pullammanappallil and Louie 1994). To perform modelization, we used only first-arrival times and we defined the spatial model resolution. This spatial resolution determines the size of the unit-cell for the model. The software calculates the cell size based on the geophone spacing (in our case 2 m) multiplied by a factor that depends on the accuracy we want for the model. In this case, the factor chosen was for the highest resolution (0.375 m), so the size of the unit-cell was  $0.375 \times 2 \text{ m} = 0.75 \text{ m}$ .

From each seismic refraction survey, we obtained a 2D  $V_p$  profile, its ray coverage and associated time fitting diagram (Fig. 4). Ray-tracing paths permit the evaluation of the model's reliability in function of ray coverage (Fig. 4c,d). The ray theory used is based on a finite difference solution of the eikonal equation solved using the fast marching method approach (Popovici and Sethian 1997). The root-mean-square (rms) error for the time fitting diagram between observed and calculated traveltimes (Fig. 4e,f), was 1.81 ms for Line 1 and 2.67 ms for Line 2. The rms error is calculated by the formula

$$E_{rms} = \sqrt{\frac{\sum_{j=1}^n (t_j^{obs} - t_j^{cal})^2}{n}},$$

where  $n$  is the number of observations,  $j$  denotes each observation and  $t_j^{obs}$  and  $t_j^{cal}$  are the observed and calculated traveltimes respectively.

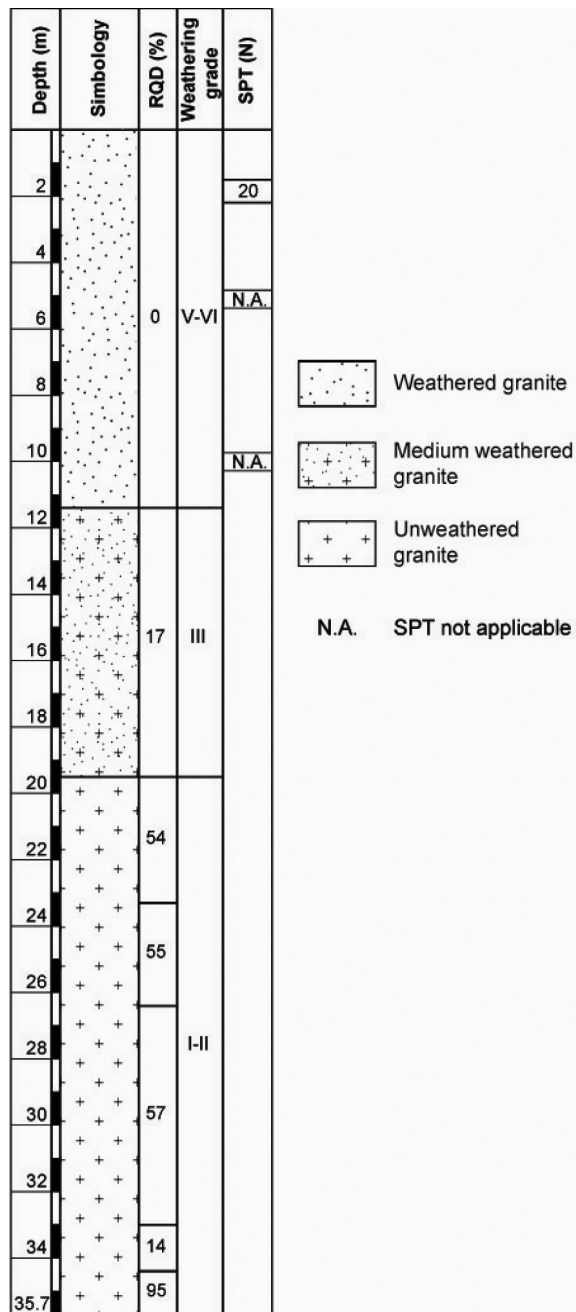


FIGURE 2

Geotechnical scheme of the borehole showing variations of the weathering grade, rock quality designation (RQD) and *SPT-N* value of granitic massifs in function of depth. *SPT-N* not applicable indicates that the *N* value is higher than 100.

### Multichannel analysis of surface waves (MASW)

The multichannel analysis of surface waves (MASW) method (Park *et al.* 1999) permits the estimation of  $V_s$  subsoil by the study of surface waves. When surface waves travel through layered media they are dispersive in nature and are controlled mainly by  $V_s$  and layer geometry (Xia *et al.* 1999). Thus, for a particular

medium the surface waves have a characteristic dispersion curve (relating phase velocity and frequency) that can be inverted to estimate  $V_s$  as a function of depth. MASW is based on the transformation of the time-offset domain of seismic data to the phase velocity-frequency domain so as to determine the fundamental dispersion curve for surface waves. The 1D profile of the  $V_s$  modelled from this curve would be situated at the centre of the geophone spread. Usually, several seismic shot records evenly spaced along the survey line are processed to construct a final pseudo 2D  $V_s$  section by spatial interpolation of 1D  $V_s$  profiles.

MASW is a relatively new method but has an ample and potentially increasing usefulness in engineering because of the possibility of the detection of velocity inversions that are usually associated with a decreased geotechnical quality in the subsoil.  $V_s$  is as valid a parameter as  $V_p$  for geotechnical characterization. However,  $V_s$  is less sensitive to saturation grade than  $V_p$ .

For the MASW method a short, pseudo 2D S-wave velocity profile was performed for each line, composed of 8 1D  $V_s$  profiles spaced 10 m apart. To acquire the data, a roll-along spreading was used, with groups of 24 geophones within the 60-geophone basic spread used in the refraction survey. The source was again the 5 kg sledgehammer strike on an aluminium plate on the ground. The optimum offset was chosen after an evaluation of the data. This suggested that 10 m assured a surface wave bandwidth range from 8–46 Hz for Line 1 and from 10–37 Hz for Line 2, which translated into a range of investigation of up to 30 m.

The processing steps include the generation of the dispersion images from seismic profiles by the wavefield transformation described in Park *et al.* (1998), the extraction of dispersion curves, the inversion of the data by the method described by Xia *et al.* (1999) and the creation of the pseudo 2D  $V_s$  section by interpolation of the inverted data. Figure 5 shows an example of each step of modelization in two of the 1D profiles. All the acquired shot records show strong surface waves such as in Fig. 5(a,b). The phase velocity–frequency images from such shot records show a good signal of dispersion curve (Fig. 5c,d), especially for frequencies lower than 25 Hz, where the signal-to-noise ratio (the estimation of the phase velocity amplitude of the desired signal with respect to other amplitudes at a given frequency) is higher. Figure 5(e,f) shows the 1D  $V_s$  profile (blue line) modelled from the fitting of the theoretical dispersion curve (black line) of the observed data (black points). The rms error between observed and calculated data was calculated for each velocity profile and was less than 6.38 m/s and 16 m/s for Lines 1 and 2, respectively. The rms error is calculated by the formula

$$E_{rms} = \sqrt{\frac{\sum_{j=1}^n (O^j - T^j)^2}{n}},$$

where  $n$  is the total number of observations,  $j$  denotes each observation and  $O$  and  $T$  are the observed and calculated phase velocities.

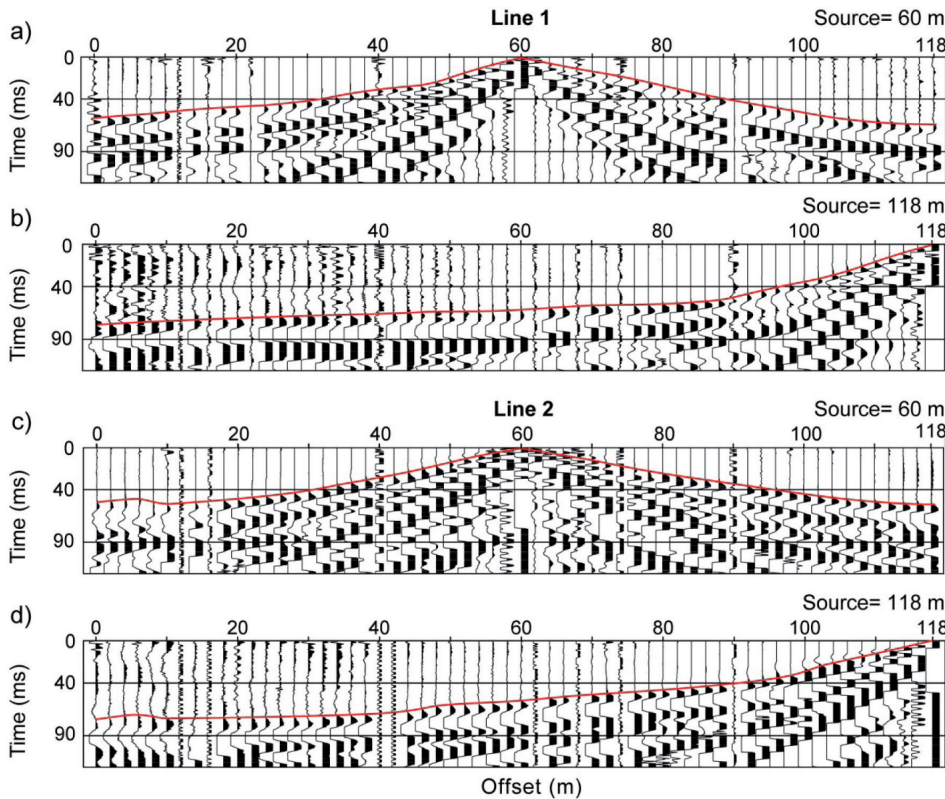


FIGURE 3 Raw seismic shot gathers with P-wave first arrivals marked in red for Lines 1 (a, b) and 2 (c, d). Source located at 60 m and 118 m.

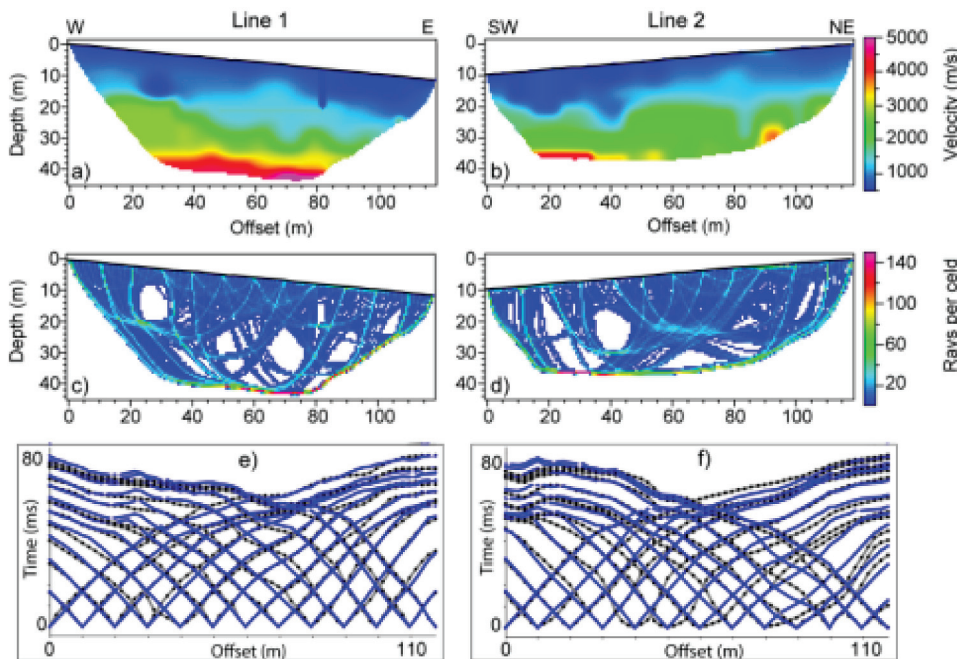


FIGURE 4 P-wave velocity models for Line 1 (a) and Line 2 (b) and colour velocity scale associated. Ray coverage for Line 1 (c) and Line 2 (d) and observed arrivals (black dots) and calculated arrivals (blue lines) corresponding to the velocity models (e, f).

Finally, after modelling the 8 1D- $V_s$  profile for each line, we generated the pseudo 2D sections (Fig. 6a,b). The software then created a section of the rms distribution (Fig. 6c,d), indicating the relative level of confidence of the velocity sections.

**Electric resistivity tomography (ERT)**

Electric resistivity tomography (ERT) is based on a material’s resistivity, a measure of how easily rocks can conduct an electric current. ERT provides a resistivity profile of the subsurface by the inversion of apparent resistivities measured in the field. Resistivity data

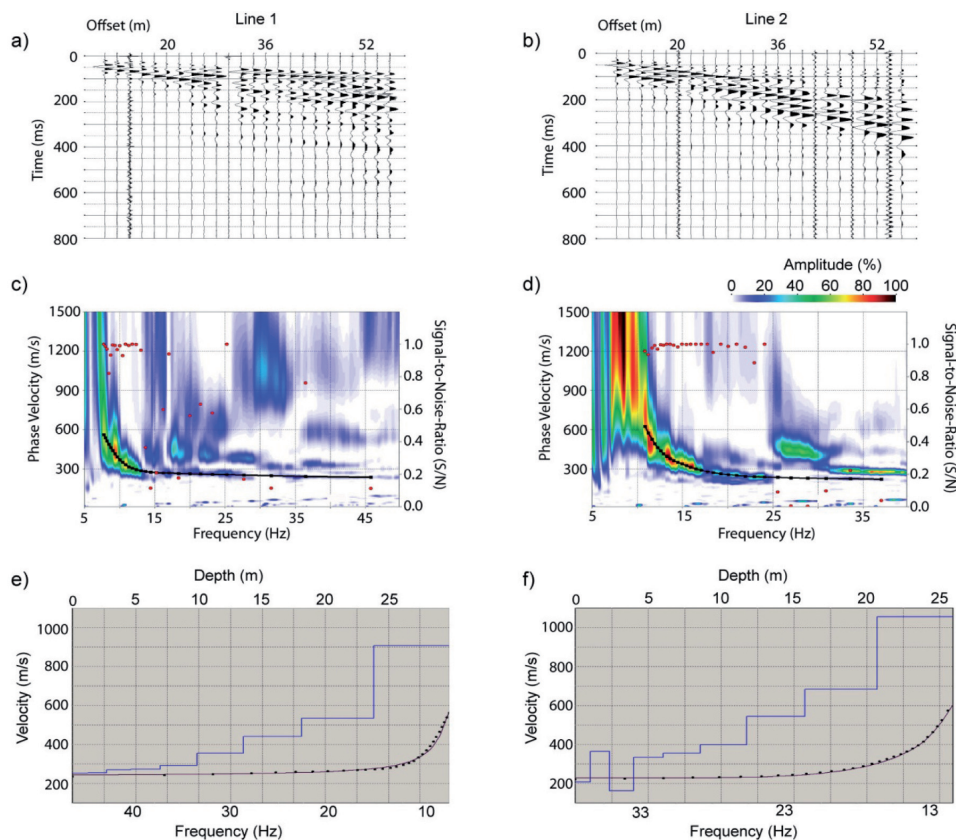


FIGURE 5

Seismic shot gathers, their corresponding phase velocity-frequency images and the resulting inverted 1D  $V_s$  profile from one shot point of Lines 1 (up) and 2 (down). In a) and b) seismic shot gathers show a strong and coherent signal of surface waves. In c) and d) the dispersion curves are marked by black squares on the phase velocity-frequency images. The red connected circles show the signal-to-noise ratio (right-hand axis) of the surface waves used to estimate the relative sensitivity of the image. Graphs e) and f) show the observed (black point) and calculated dispersion curves (black line) and the modelled  $V_s$  profile (blue line). The lower axis shows the frequency of the dispersion curve data and the upper axis shows the depth of velocity profile.

are derived through a quadripole geometry where two poles inject current into the ground and the resulting potential is measured by the other two electrodes. The resistivity values depend mainly on the composition of the materials, their porosity, grade of fracturation and weathering, the saturation state and the type of fluid saturation. As in seismic velocities, an increase in resistivity normally means higher quality terrain. However, changes on humidity content are capable of producing large variations in resistivity, so caution must be taken when interpreting ERT values alone.

ERT acquisition was performed with an AGI SuperstingR8 and 56 electrodes spaced 3 m apart. In order to control the lateral heterogeneities in the rock massif, a dipole-dipole arrangement was selected. On acquisition, two 'stack' or injections per measurement were made for 762 quadripoles. The difference in values between stack injections gives us an idea of the quality of the field data, which in our case was good, with 90% of our measurements displaying an error lower than 0.4% and 100% below 1.1%.

The software used for modelization involved data inversion based on Occam's inversion (Constable *et al.* 1987; deGroot-Hedlin and Constable 1990), which is also known as smooth inversion. In the modelization process the initial model used was the profile of apparent resistivity obtained in the field. Adjustment between observed and calculated apparent resistivity was good, with an rms error of 3.55% for Line 1 and 2.45% for Line 2. The rms is calculated by the formula

$$RMS = \sqrt{\frac{\sum_{j=1}^n \left( \frac{d_j^{cal} - d_j^{obs}}{d_j^{obs}} \right)^2}{n}} 100,$$

where  $n$  is the total number of observations,  $j$  denotes each observation and  $d^{cal}$  and  $d^{obs}$  are the calculated and observed data.

### LABORATORY TESTS

The laboratory tests cover the measurement of the ultrasonic seismic velocities, density and open porosity of the core samples representative of all the granite weathering grades, from sandy soil to rock. However, we need to keep in mind that there is an implicit bias in the selection of the test samples towards less altered ones, especially in the shallow sandy level of the granite. In this level we could only take one undisturbed sample at 2.5 m depth.

As  $V_p$  depends on the rock humidity, which was altered by drilling, rock was tested in dry and saturated conditions to evaluate its influence. However, in the field, the water table is below our geophysical maximum depth investigation so field data can be easily assimilated to the dry state.

The rock sampling interval was one metre from 11.4–35.7 m depth. The samples were cylindrical, with lengths between 8.7–12.6 cm. Originally we planned a length of 12 cm for all the samples but in some cases fracturation of the massif forced shorter samples. Open porosity was calculated by the hydrostatic

weight method. The acquisition of ultrasonic velocities was made with an OYO Sonicviewer. The measurements were made with transducers with a nominal frequency of 45 kHz for the P-waves and 33 kHz for the S-waves.

## RESULTS

In the following section we show the results with the three geophysical methods and the laboratory test. For Line 1, we compared the borehole data with the corresponding depth  $V_p$ ,  $V_s$  and resistivity values in order to define various levels of weathered rock. In Line 2, with no direct data available, the levels defined for Line 1 conform the basis for its interpretation. Both results are then correlated with the measurements obtained in the laboratory from the borehole samples.

Various considerations regarding the interpretation of the geophysical models for Line 1 need to be pointed out. All parts of Fig. 7(a–d) share the same vertical and horizontal scale (1:1). For the  $V_p$  model (Fig. 7a), the resistivity model (Fig. 7c) and the comparison between interpretations (Fig. 7d), the far west of the resistivity model has been taken as zero depth. In the case of the  $V_s$  model (Fig. 7b), the processing software created a 2D flat profile (whose surface is the zero depth) where the topography of the study area is not taken into account. In order to be able to compare this model with the others (Fig. 7d), a topographic correction was applied to the  $V_s$  interfaces, in addition to taking the far west profile as the zero depth reference. The additional  $V_s$  limit in Part d corresponds to the lower limit of the  $V_s$  model (Part b).

The same was done for Line 2 (Fig. 9) as for Line 1. In this case, however, the north-east corner of the resistivity model was taken as the zero depth.

## FIELD DATA RESULTS

### Line 1

The  $V_p$  model for Line 1 shows a range of velocities between 477 m/s at the surface and 5500 m/s at 42 m (Fig. 7a). The interfaces interpreted match with those observed through the borehole with depth differences lower than  $\pm 2$  m. P-wave velocities lower than 1000 m/s and between 1400–1450 m/s correlate with weathering classes V–VI and III, respectively. At 39 m depth in

the central part of the line, there is a significant velocity increment from 2600–3100 m/s to 4100–5500 m/s indicating the improvement of the massif quality with depth. Borehole samples confirm this as granite class I–II and an increment in rock quality designation with depth from 54–95 %.

The obtained MASW model shows  $V_s$  between 230–1166 m/s up to a maximum depth of investigation of 30 m (Fig. 7b). Three main velocity intervals or layers have been correlated to different weathering grades. As with the  $V_p$  model, two shallow intervals of velocities, the first between 230–297 m/s and the second between 375–528 m/s, indicate granite classes V–VI and III, respectively. The highest velocities of 600–1166 m/s belong to the fresh granite (class I–II). These velocities increased with increasing depth, at the same time that fracturation decreased (rock quality designation of 54–57 %).

The resistivity section shows values from 66–3125  $\Omega\text{m}$  down to 41 m depth (Fig. 7c). An initial interpretation relates resistivities of 60–500  $\Omega\text{m}$  and 500–800  $\Omega\text{m}$  with high to medium weathered rock and those from 800–3125  $\Omega\text{m}$  with fresh rock. Borehole samples confirm that resistivities higher than 800  $\Omega\text{m}$  are observed in rock class I–II. However, borehole data relate resistivity values between 66–800  $\Omega\text{m}$  with weathered granite class III–VI but do not allow us to differentiate grades as accurately as seismic velocities do. In this case, the wide range of resistivities of weathered granite (66–800  $\Omega\text{m}$ ) implies that near-surface resistivities become sensitive to other factors such as humidity or clay content. Probably the lowest resistivities, those close to 66  $\Omega\text{m}$ , indicate extreme degradation of the rock massif involving the partial transformation of the granitic minerals to clay (granulometric analysis confirmed at least 8% of silt-clay particles). This suggests that the limit initially interpreted, between resistivities above and below 500  $\Omega\text{m}$ , has no direct relation to the degree of alteration of the granite. Because of this we excluded this limit from the comparison between interpretations (Fig. 7d).

Also, at the beginning of the profile, inside the low resistivity level there are several zones with values higher than 1200  $\Omega\text{m}$ , corresponding to class I–II. These values are interpreted as fresher granite boulders inside a highly weathered granite matrix. The presence of these ‘boulders’ has not been confirmed by

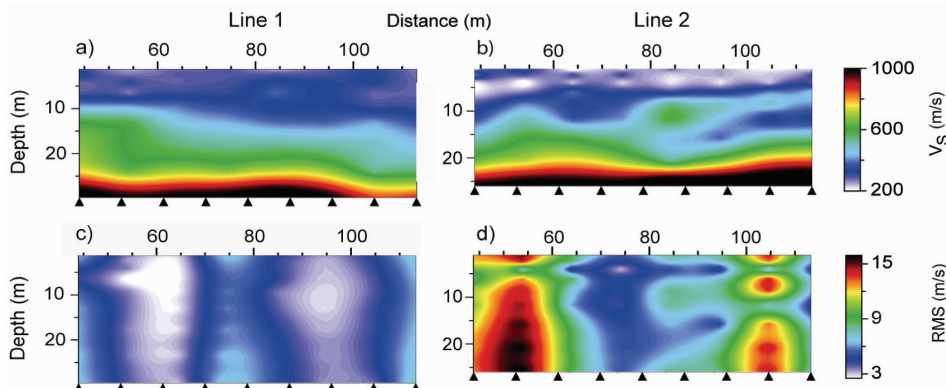


FIGURE 6 a) and b) show the 2D  $V_s$  pseudo-section of Lines 1 and 2 with the related rms error pseudo-section in (c) and (d). Black triangles show the situation of the 1D  $V_s$  and rms profiles used to construct pseudo-sections.

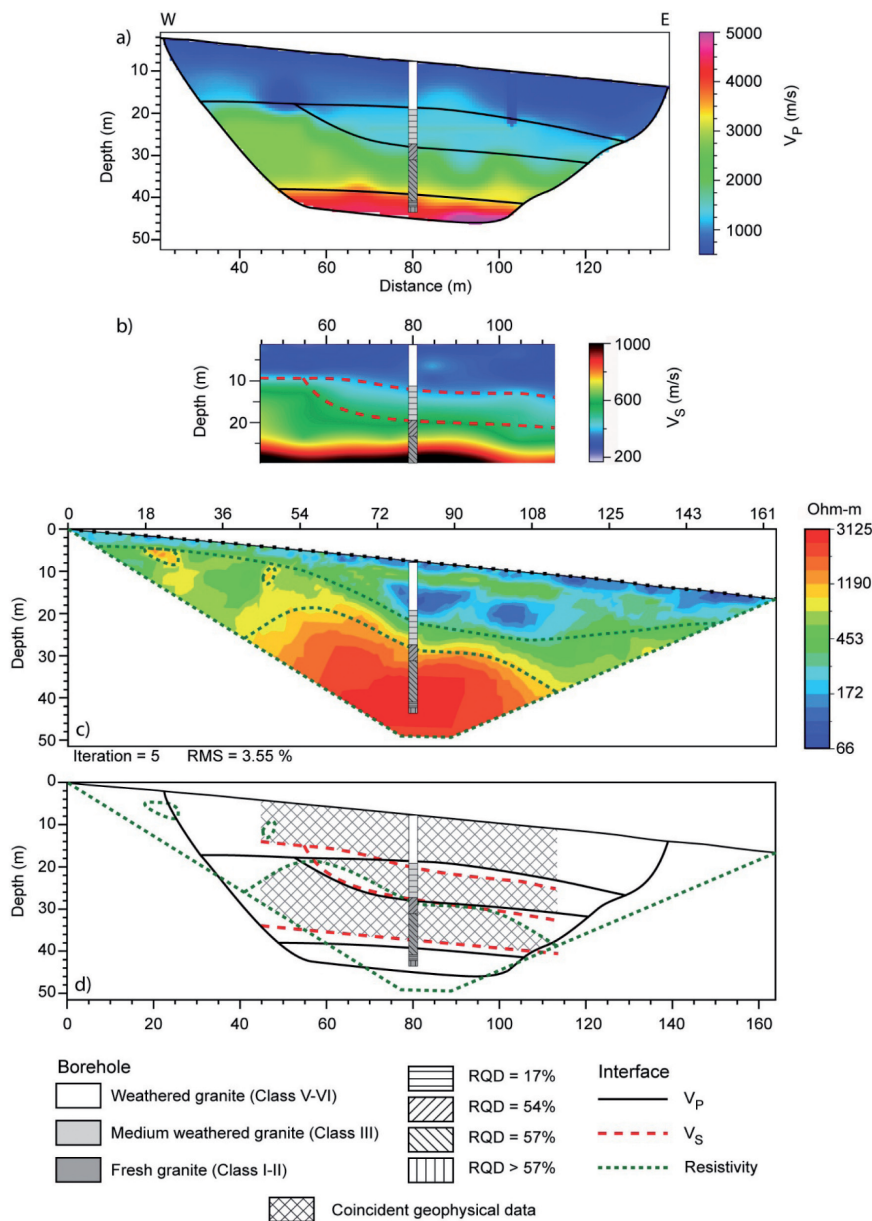


FIGURE 7

$V_p$  (a),  $V_s$  (b) and resistivity (c) geophysical models and interpreted interfaces of Line 1. d) This shows a joint comparative of three geophysical results for including the geotechnical data from the borehole. A hatched pattern is shown when the three field methods agree in their interpretations, mainly in the better-sampled central part of section.

boreholes but this interpretation is based on similar features observed in the outcrops near the study lines.

The next step in the study was the joint interpretation of the geophysical models and borehole data (Fig. 7d). We compared all interfaces and geophysical values with the geological data to obtain a final, well-constrained, accurate geotechnical model of the subsoil (Fig. 8 and Table 2). In the subsoil profile we have emphasized the areas with reliable information, which are those where the geophysical data interpretation agrees in the three methods employed.

$V_p$  and  $V_s$  show two upper levels with low velocities related to weathering classes V–VI and III dipping to the south-west. Granite class III shows a rock quality designation of 17% due to the massif alteration and tapering to the west. The depth differ-

ence of the interfaces is up to 3m in this area but is smaller in the centre of the line, where coverage is higher. The limit interpreted in the resistivity section between fresh and weathered rock matches those obtained in the  $V_p$  and  $V_s$  models well, especially in the central part of the study area. Low resistivity values from 66–800  $\Omega$ m correspond with low  $V_p$  and  $V_s$  related to weathered granite classes III–VI. The good lateral resolution of the method has allowed us to interpret fresh granite boulders inside the weathered matrix class V–VI, which the seismic velocities apparently averaged with the raypaths.

Higher  $V_p$ ,  $V_s$  and resistivities are related to fresh rock (class I–II) affected by different fracturation grades. The contact between fresh and weathered rock is sharp at the beginning of the line in the west and becomes more gradual in the middle and

towards the east. The subdivisions made in fresh granite are only based on seismic velocities, since resistivity values do not show significant changes. Although the rock quality designation values do not match with the geophysical interfaces, the lower weathering grade suggests that the velocity gradient at depth for  $V_p$  and  $V_s$  is governed by fracturation, with the weathering effect becoming a secondary factor in the velocity results. The deepest level of fresh rock is distinguished by the high  $V_p$  of 4400– 5500 m/s. At this level, the good quality of the final core samples of the borehole and the higher  $V_p$  both indicate a low fractured massif with an estimated rock quality designation > 57%.

The correlation between geophysical and geotechnical parameters is good for more than 40% of the total line length, which can be used confidently in the interpretation of Line 2, (see next section), where no direct borehole data were obtained.

**Line 2**

The  $V_p$  model shows a range of seismic velocities with values from 518 m/s at the surface to 4315 m/s at 38 m (Fig. 9a). Three levels were defined, as in Line 1, with velocities of 518– 1200 m/s, 2000–2450 m/s and 3320–4315 m/s. Based on the results of Line 1, the upper low-velocity level has been interpreted as highly weathered granite class V–VI. The second level (2000– 2450 m/s)

represents slightly lower velocities than those correlated with fresh rock (class I–II with rock quality designation = 54–57) and higher than the ones obtained for class III rock with rock quality designation = 17. This is probably because this granite is in one of the multiple intermediate states of weathering between both cases. Thus, the estimated weathering class is II–III, with a rock quality designation of 24–66 %. High velocity zones of 3320– 4315 m/s at the beginning and end of the line indicate fresh granite class I–II with an estimated rock quality designation  $D > 54\%$ .

The MASW model shows a  $V_s$  range from 264 m/s at the surface to 1150 m/s up to a depth of 25m (Fig. 9b). The lowest velocities of 264–420 m/s are interpreted as highly weathered granite class V–VI at 11–25 m depth. Inside this level the model shows a higher velocity zone of 550–600 m/s between the central part and the end of the line, which suggests a localized area of granite class I–II inside a highly weathered matrix. Higher velocities from 540–1150 m/s belong to fresh rock (class I–II) with a rock quality designation of 17–54%.

As with the resistivity model for Line 1, the section of Line 2 shows lateral changes in resistivity and an equal maximum depth of investigation of 41m (Fig. 9c). The principal difference between both profiles is the wider resistivity range in Line 2, ranging from a lowest value of 65  $\Omega m$  to the highest one at

TABLE 2  
Correlation between field geophysical data and geotechnical data from the borehole in Line 1

Type	Description	Weathering grade	Rock quality designation	$V_p$ (m/s)	$V_s$ (m/s)	Resistivity ( $\Omega m$ )
1	Granite converted to sandy soil	V–VI	0	600–1000	230–297	66–800
2	Granite fully or partially weathered to soil	II–IV	17	1400–1450	275–528	
3	Fresh rock	I–II	54–57	2600–3100	600–1166	800–3125
4	Fresh rock	I–II	>57	4100–5500	–	

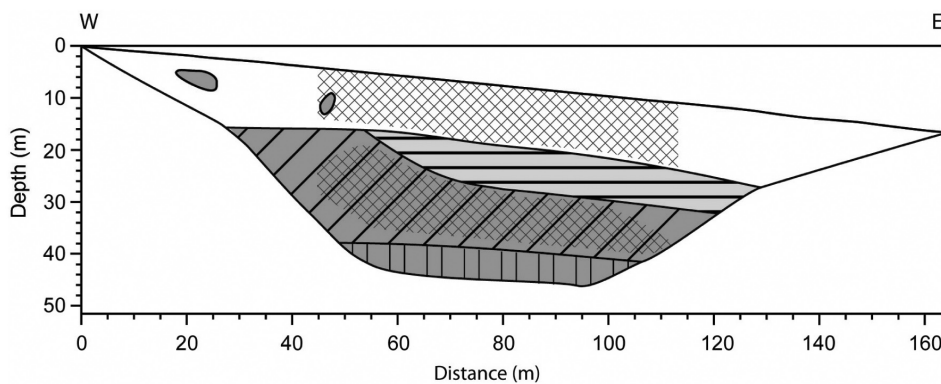


FIGURE 8  
Final geotechnical interpretation of Line 1 based on both geophysical and geotechnical data. The figure shows the three interpreted levels of weathering grade, together with the rock quality designation of each one level. The hatched pattern shows when the three field methods agree in their interpretations.

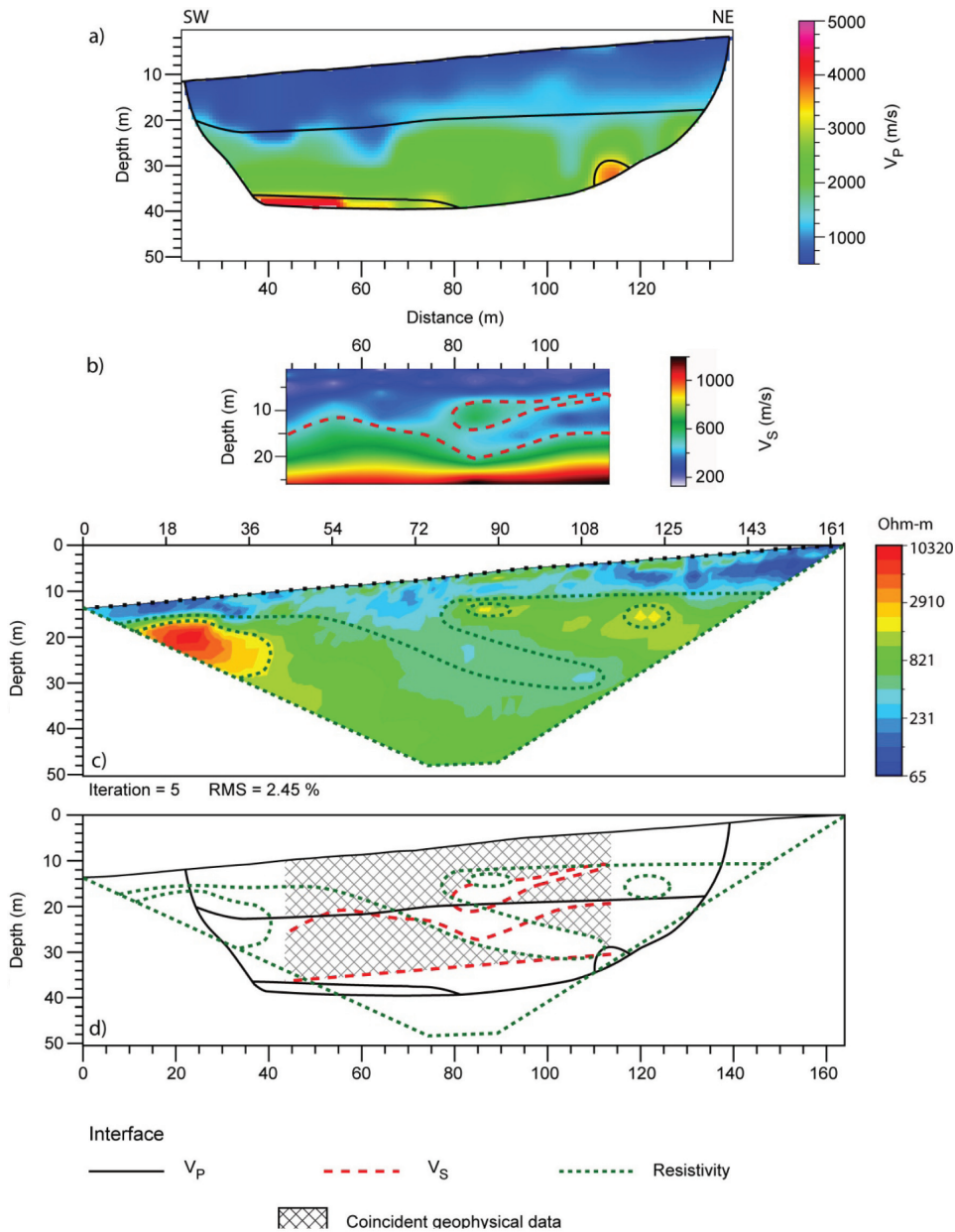


FIGURE 9  $V_p$  (a),  $V_s$  (b) and resistivity (c) geophysical models and interpreted interfaces of Line 2. d) This shows a joint comparative of three geophysical results. A hatched pattern is shown when the three field methods agree in their interpretations.

10–320  $\Omega\text{m}$ . Although high resistivities for Line 2 are higher than for Line 1, the resistivity section shows a generalized low resistivity range from 65–900  $\Omega\text{m}$  with located maxima of 1200  $\Omega\text{m}$  (87 m and 123 m), or 1700–10320  $\Omega\text{m}$  (12–39 m). Following the baseline obtained for Line 1, these configurations indicate that the granite massif studied is generally weathered (class III–VI), except for some located zones of fresh rock (class I–II). There is a significantly low resistivity of 65–500  $\Omega\text{m}$  over the first 10 m, which could indicate a higher degree of alteration descending to 28 m in the middle of the study area.

All the geophysical data were compared in Fig. 9(d) to define subsoil levels with  $V_p$ ,  $V_s$  and resistivity attributes and then each one was correlated with geotechnical parameters based on Line 1 observations.

$V_p$  and  $V_s$  interpreted sections have some matches and some differences for the same study area. Both sections show a shallow layer, with low velocities corresponding to a highly weathered granite class V–VI and an increment in velocities related to a decrease in weathering grade. However, the  $V_p$  profiles only show a velocity increment with depth, whilst the  $V_s$  section delineates a velocity inversion in the centre of the line, inside the low velocity level. This velocity inversion is interpreted as showing the presence of fresh rock inside the weathered matrix. Other differences between  $V_p$  and  $V_s$  models arise from the range of values for the high velocity layer.  $V_p$  suggests a granite weathering class II–III, whilst  $V_s$  corresponds to the range of a class I–II fresh rock.

In the resistivity section, shallow low-resistivity values have

been related to a possible highly weathered granite that extends down deeper in the middle part.  $V_s$  interpretation shows a similar response, although without reaching exactly the same depth. In the same area, the local high resistivity values match the higher S-wave velocity. This configuration supports the interpretation of a shallow granite class V–VI that extends deeper in the central part of the line, with local zones or boulders of fresher rock embedded in it.

As observed in Line 1,  $V_p$  and  $V_s$  in Line 2 show higher values with depth relating to medium to low weathered granite, a fact that yields no apparent expression in the resistivities. The  $V_p$  velocities of 2000–2450 m/s are slightly lower than the ones for fresh rock in Line 1. The fact of a generalized lower resistivity than the one defined for fresh rock in Line 1 suggests, together with  $V_p$  values, that this time the granite is somehow more affected by alteration. Joint resistivity,  $V_p$  and  $V_s$  data lead us to conclude that the weathering grade is intermediate between fresh rock to partially altered (class II–III with rock quality designation of 17–54%). The fresh rock for this line is inferred from resistivities higher than 1200  $\Omega\text{m}$  located along the study area. A  $V_p$  zone of 3320–4315 m/s could indicate fresh rock but low resistivities at the same depth suggest the opposite.

The final geotechnical model is characterized by a generalized higher degree of alteration than in Line 1 (Fig. 10 and

Table 3). The two main features are a shallow area of granite class V–VI and a poor to medium weathered granite (class II–III) beneath. Fresh rock (class I–II) appears in local zones related principally to high resistivities, as well as to a high  $V_p$ . Low resistivity for the central part of the line suggests that the altered rock class V–VI continues down to 28 m, however there is no support for this from  $V_s$  and  $V_p$  (see regular question mark in Fig. 10). For the granite with a  $V_p$  of 2000–2450 m/s and a  $V_s$  of 540–1150 m/s, we have estimated a weathered class II–III and a rock quality designation between 17–54%. Fresh granite only appears in local areas inside the weathered granite. The main criteria to identify fresh granite are resistivities higher than 1200  $\Omega\text{m}$  similar to those at the beginning of the line. A second criteria, although less robust because there is no support from high resistivities (see bold question mark in Fig. 10), would be  $V_p$  velocities of 3320–4315 m/s. The rock quality designation for fresh rock calculated by both criteria is higher than 57%.

**LABORATORY DATA RESULTS**

Weathering grade, density and open porosity of core samples show a clear relationship (Fig. 11a,b). The lowest density is that of the sandy soil sample at 2.5 m depth (class V–VI), with a value of 2.02 g/cm<sup>3</sup>. The density and open porosity vary gradu-

TABLE 3  
Estimated correlation between geophysical and geotechnical data in Line 2

Type	Description	Weathering Class	Rock quality designation (%)	$V_p$ (m/s)	$V_s$ (m/s)	Resistivity ( $\Omega\text{m}$ )
1	Highly weathered granite	V–IV	0	518–900	264–420	65–900
2	Poor to medium weathered granite	II–III	17–54	2000–2450	540–1150	
3	Fresh granite	I–II	>57	–	–	1200–10320
4	Fresh granite	I–II	>57	3320–4315	–	–

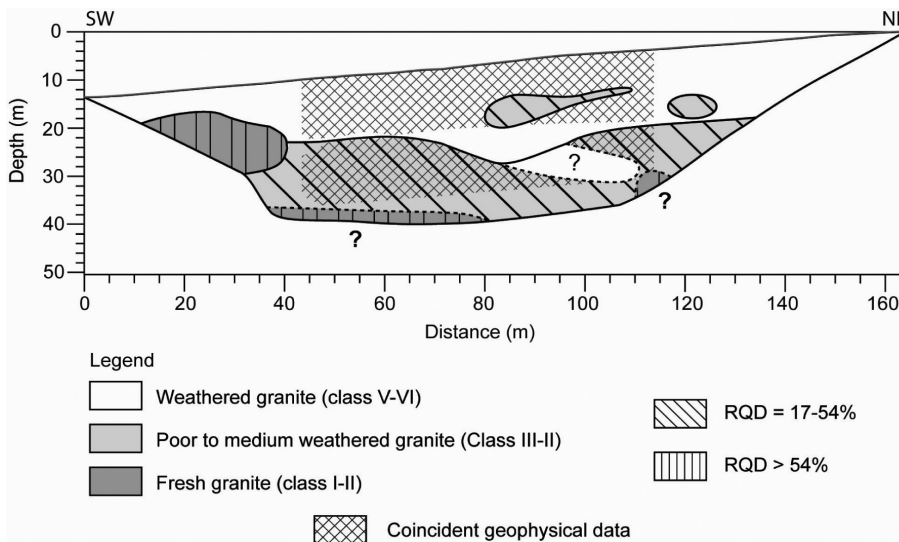


FIGURE 10  
Final interpretation of Line 2. The weathering grade class and rock quality designation values of three levels are estimated comparing the geophysical data of Line 2 with the previous correlation between the geophysical and the geotechnical data of Line 1. The question marks indicate areas (delimited by dotted lines) where interpretations of different methods are contradictory. The hatching shows the area where all three methods agree.

ally in depth from 2.51 g/cm<sup>3</sup> and 5.1 %, respectively, for highly weathered samples, to 2.66 g/cm<sup>3</sup> and 0.2%, respectively, for fresh granite. The weathered rock samples are in a depth range of 11–19 m, coinciding with class III of the rock massif and sporadically at depths of 23 m and 33 m. The density range, 2.61–2.66 g/cm<sup>3</sup> and the open porosity, 0.2–0.5% for fresh rock of massif class I–II, are narrower than those of the weathered samples. There is an isolated case at 20 m where a sample of endoskarn shows a highest value of density with a relatively high porosity compared to fresh granite.

The seismic velocities in the laboratory are influenced by the alteration state of the samples (Fig. 12 a,b). The  $V_p$  and  $V_s$  decrease with increasing weathering grade from  $V_p$  5774 m/s and  $V_s$  3045 m/s for fresh rock class I–II and to 379 m/s and 111 m/s for samples of sandy soil or granite class V–VI. As shown in Fig. 12 (c,d), seismic velocity decreases proportionally with density and inversely to open porosity.

Dry and saturated test velocities indicate a higher sensitivity of  $V_p$  to saturation state with respect to  $V_s$ , which does not vary so significantly. Figure 12(a,b) shows higher  $V_p$  values for the saturated state of the sample, whilst  $V_s$  is similar in both states. The water influence on  $V_p$  is very clear when we look at the trend with depth of both dry and saturated  $V_p/V_s$  ratios (Fig. 12e). Higher  $V_p/V_s$  ratios respond to weathered samples of class V–VI and class III, which decrease in depth as does open porosity (Fig. 11b). This fact suggests that open porosity and  $V_p/V_s$  ratios are related ( $V_p/V_s$  decreases proportionally with open porosity) and could be used as joint criteria in a field geophysical survey (Fig. 12f). The differ-

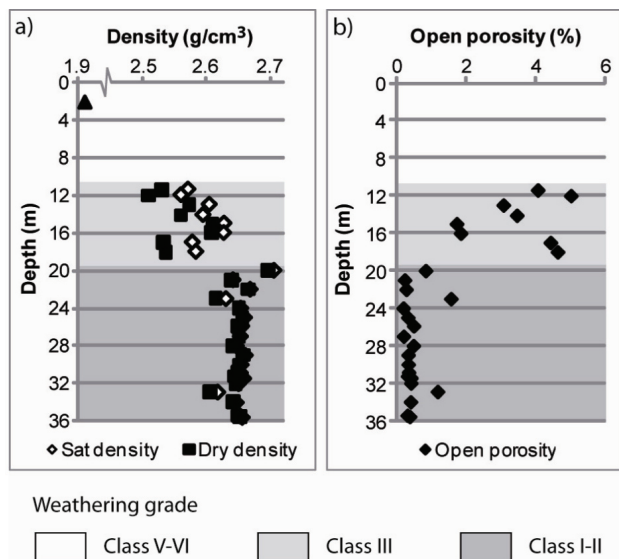


FIGURE 11

Density (a) and open porosity (b) tested in the laboratory on borehole samples as a function of depth. Density has been measured for weathered granite converted into soil (dark triangles) and for saturated (empty diamonds) and dry (black squares) rock samples. Density increases while open porosity decreases with a decreasing granite weathering grade.

ences between dry and saturated state are mainly due to water influence on  $V_p$ . For rock class I–II, the water influence on  $V_p$  is low and the dry and saturated  $V_p/V_s$  ratio differences only become noticeable in the rock matrix features. As shown in Fig. 12(g), the  $V_p/V_s$  ratio decreases inversely to density.

The comparison between field and laboratory seismic velocities shows similar values for weathering granite class V–VI, while differences become higher for granite class I–II (Fig. 12a,b). This could be explained because the seismic velocity of sandy soil at the surface in the field only depends on its density, as is the case in the laboratory. While the laboratory velocities of the samples depend on the matrix features, the field velocities are subjected to other scale factors such as massif fracturation or percentage of weathering, both of which have the effect of lowering them. In addition, the laboratory velocities show the influence of the rock matrix, weathered up to 19.5 m depth, which confirms that low field velocities of granite class III are principally due to rock weathering. On the other hand, the generalized high laboratory velocities of granite class I–II suggest that the difference with the field velocity is an expression of the fracturation.

The  $V_p/V_s$  ratio shows a range of values and a similar trend for weathered granite (class V–VI and III) in both the field and the laboratory. In the case of fresh rock, however, field values display the opposite trend to laboratory ones. This indicates that laboratory data can predict the general field behaviour of  $V_p/V_s$  for shallow weathered levels but not for the deepest level of fresh rock.

Elastic parameters like the Poisson's ratio, or Young, shear and bulk moduli, were calculated based on both laboratory and field data. The Poisson's ratio is directly related to  $V_p$  and  $V_s$  and shows the same behaviour as the  $V_p/V_s$  ratio in the field and the laboratory (Fig. 13a). The laboratory and field Poisson's ratio decreases with decreasing alteration grades, except for fresh rock. As we saw with the seismic velocities, the Young, shear and bulk moduli calculated from the field data and the laboratory data are similar for granite class V–VI but are underestimated for granite class III and especially for class I–II (Fig. 13b–d). This is due partly to the fact that for practical purposes laboratory samples are always chosen from those with least weathering, and partly to the fracturation of the massif, which at a laboratory scale is neglected.

Even taking those limitations in account, elastic constants for the fresh rock calculated from field velocities are too low (being similar to sediment values) and cannot be explained merely as an effect of fracturation and/or weathering. The origin of unrealistic  $V_p/V_s$  and elastic constants for fresh rock seems to arise from the low velocity of S-waves with respect to P-waves. Table 4 shows laboratory and field  $V_p/V_s$  ratios and elastic constants calculated for the different levels of weathering inside the granitic massif.

## DISCUSSION AND CONCLUSIONS

A granite massif in north-west Spain with various lateral and depth weathering variations was studied by field and laboratory geophysical methods to provide a geologically and geotechni-

cally useful characterization. The field approach involved a multi-technique approach in which different methods increased their individual reliabilities when carried out together.

The variations of  $V_p$ ,  $V_s$  and resistivity values obtained in the field have been related to changes in the fracturation and weathering grade of the granitic massif. Seismic velocities are especially sensitive to both variables. Resistivity seems to be a little more limited when distinguishing weathering levels but solves the presence of local fresh boulders embedded inside the weathered matrix, an issue that seismic velocities are not able to discern. The joint interpretation of geophysical and geotechnical methods has allowed the characterization of the Carlés massif, which in turn has allowed us to define various levels with their own characteristics based on engineering classifications such as Brown (1981) or

rock quality designation. The joint interpretation of the field geophysical data has allowed us to generate a more accurate geotechnical model. The model offers higher resolutions than with separate interpretations. It has differentiated areas with high reliability where all the geophysical data agree and areas of more doubtful information, which could afterwards be drilling targets.

The laboratory test of granite samples has allowed us to predict the behaviour of seismic velocities in different degrees of rock weathering. Both field and laboratory velocities decrease with increased weathering but show a different range of values. The disagreements in velocities are more significant in fresh rock as a result of the use of non-fractured rock in the laboratory. For sandy soil however, velocities are comparable and similar since they depend only on soil characteristics.

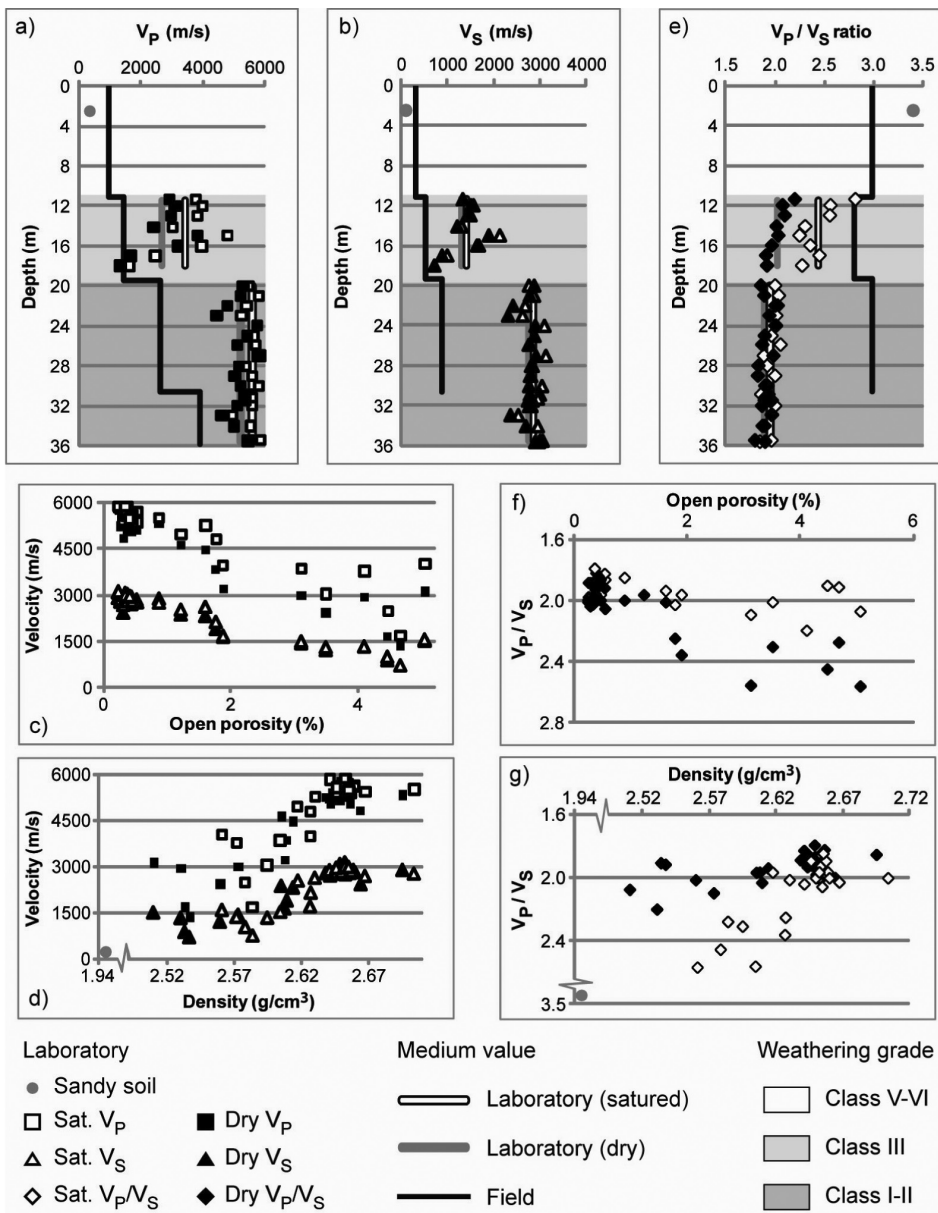


FIGURE 12 Laboratory and field  $V_p$ ,  $V_s$  and  $V_p/V_s$  values as function of depth (a, b, e), open porosity (c, f) and density (d, g). The laboratory data are calculated from core samples of granite weathered to soil (grey point) and rock samples that are saturated (empty square, triangle and diamond) and dry (black square, triangle and diamond). The arranged values have been calculated for laboratory samples of saturated (empty line) and dry rock (grey line) and for field data (black line). All the data are compared with the weathering grade of the granite observed in the borehole.

TABLE 4

Comparison between granite weathering grade and rock quality designation observed in the borehole with calculated laboratory (up) and field (down)  $V_p/V_s$  ratios and elastic constants for Line 1

Weathering grade and rock quality designation	$V_p/V_s$	Poisson	Young (GPa)	Strain (GPa)	Bulk (GPa)
V–VI	3.40	0.45	0.07	0.02	0.24
	3.00	0.44	0.61	0.21	1.62
III (17)	2.03	0.34	13	5	14
	2.81	0.43	1.95	0.68	4.46
I–II (54–57)	1.90	0.31	52	20	46
	2.98	0.44	5.90	2.05	15.53

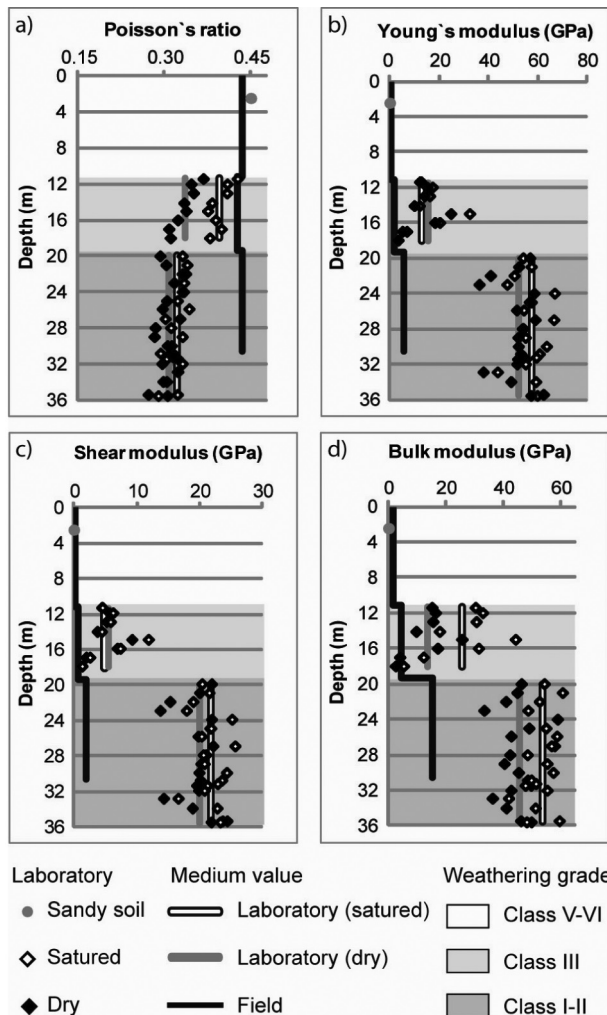


FIGURE 13

Field and laboratory Poisson's ratio (a) and Young (b), shear (c) and bulk (d) moduli. The laboratory data are calculated from core samples of granite weathered to soil (grey point) and rock samples that are saturated (empty diamond) and dry (black diamond). The arranged values have been calculated for laboratory samples of saturated (empty line) and dry rock (grey line) and for field data (black line). All the data are compared with the weathering grade of the granite observed in the borehole.

The  $V_p/V_s$  ratio and elastic parameters calculated from field and laboratory velocities are once again similar in trend and value for weathered granite but are very different for fresher rock, especially for the values obtained in the field, where the fresh rocks approached values of a complete altered one. The cause for this anomaly may be attributed to the low values observed in the  $V_s$ , which makes the difference between both velocities unrealistic. The anomalies in the values of seismic velocity have been described in seismic refraction applications by Ivanov *et al.* (2005a,b) and have also been described when using surface waves by Dal Moro (2008). According to these authors, the inverse refraction and dispersion curve problem does not have a unique solution uncertainty, because of which there is a range of uncertainty for the velocity values. This increases with depth and is even bigger for the MASW method, which adds fresh ambiguity due to the low resolution in the dispersion curve when dealing with low frequencies (which provide information about the deeper layers). Thus, the reason for the disagreements and anomalies in the fresher rock may be methodological and the elastic parameters calculated based on those velocities are probably unrealistic.

The aim of the study is to demonstrate the benefits of the joint use of seismic refraction, MASW and ERT methods to characterize and to calculate elastic parameters of a weathered granitic massif. We conclude that the joint use and interpretation of the three methods employed in this pre-doctoral study is an excellent tool for providing a full characterization of a weathered rock massif. It is easy, quick and economically feasible when studying large areas. Joint interpretation provides several advantages when compared to traditionally separate approaches, which can be beneficial in fields such as engineering, geology or hydrogeology. It makes the interpretation of geophysical data easier, improves the spatial resolution of single interpretation and allows us to compare the uncertainty in the depth of interpreted interfaces. However, care must be taken when trying to calculate elastic parameters based on field seismic refraction and MASW velocities, especially at depth, where ambiguity in velocities may cause invalid results.

A future line of research will be centred on consolidating this methodology to calculate elastic parameters of the subsoil. We need to confirm if this is valid for other geological environments. We also need to compare the data obtained in seismic refraction

and MASW with higher-resolution seismic methods, such as cross-hole and downhole to evaluate the difference between velocities. Based on this, it may be profitable to work with the joint inversion of refraction and MASW data in order to arrive at a realistic solution, a solution that would be more accurate than in both methods separately.

#### ACKNOWLEDGEMENTS

The present work has been supported by the project MFOM-06-1 funded by the Ministry of Public Works of Spain (National Programme of Construction, R&D National Plan 2004-2007) and by the Consolider-Ingenio 2010 Programme under Project 'Topo-Iberia' CSD2006-0041. During this work Javier Olona enjoyed a PhD grant awarded by the Ministry of Education and Science. We are grateful to Santiago González from the company Kinbauri Spain (Orvana Minerals Corp.) and Dr Lope Calleja from the Department of Geology of the University of Oviedo for their help during field and laboratory works. We want to express our gratitude to Julian Ivanov from the Kansas Geological Survey for his constructive comments in preparing this manuscript. We thank Robin Walker (BSc) for his revision of the English in the final manuscript. We also thank the reviewers for their comments, which have helped us to improve the manuscript.

#### REFERENCES

- Begonha A. and Sequeira Braga M.A. 2002. Weathering of the Oporto granite: Geotechnical and physical properties. *Catena* **49**, 57–76.
- Benson R.C., Yuhr L. and Kaufmann R. 2003. Some considerations for selection and successful application of geophysical methods. 3<sup>rd</sup> International Conference on Applied Geophysics, Geophysics 2003, 8–12 December, Orlando, Florida, USA, Expanded Abstracts.
- Bohachevsky I.O., Johnson M.E. and Stein M.L. 1986. Generalized simulated annealing for function optimization. *Technometrics* **28**, 209–217.
- Brown E.T. 1981. *Rock Characterization, Testing and Monitoring: ISRM Suggested Methods*. Pergamon Press.
- Constable S.C., Parker R.L. and Constable C.G. 1987. Occam's inversion: A practical algorithm for generating smooth models from electromagnetic sounding data. *Geophysics* **52**, 289–300.
- Dal Moro G. 2008.  $V_s$  and  $V_p$  vertical profiling via joint inversion of Rayleigh waves and refraction traveltimes by means of bi-objective evolutionary algorithm. *Journal of Applied Geophysics* **66**, 15–24.
- DeGroot-Hedlin C. and Constable S. 1990. Occam's inversion to generate smooth, two-dimensional models from magnetotelluric data. *Geophysics* **55**, 1613–1624.
- Dewandel B., Lachassagne P., Wyns R., Maréchal J.C. and Krishnamurthy N.S. 2006. A generalized 3-D geological and hydrogeological conceptual model of granite aquifers controlled by single or multiphase weathering. *Journal of Hydrology* **330**, 260–284.
- Fazzito S.Y., Rapalini A.E., Cortés J.M. and Terrizzano C.M. 2009. Characterization of Quaternary active faults by electric resistivity tomography in the Western Precordillera of Mendoza and San Juan, Argentina. *Journal of South American Earth Sciences* **28**, 217–228.
- Friedel S., Thielen A. and Springman S.M. 2006. Investigation of a slope endangered by rainfall-induced landslides using 3D resistivity tomography and geotechnical testing. *Journal of Applied Geophysics* **60**, 100–114.
- Ivanov J., Miller R.D., Lacombe P., Johnson C.D. and Lane Jr J.W. 2006. Delineating a shallow fault zone and dipping bedrock strata using multichannel analysis of surface waves with a land streamer. *Geophysics* **71**, A39–A42.
- Ivanov J., Miller R.D., Xia J., Steeples D. and Park C.B. 2005a. The inverse problem of refraction traveltimes. Part I: Types of geophysical nonuniqueness through minimization. *Pure and Applied Geophysics* **162**, 447–459.
- Ivanov J., Miller R.D., Xia J., Steeples D. and Park C.B. 2005b. The inverse problem of refraction traveltimes. Part II: Quantifying refraction nonuniqueness using three-layer model. *Pure and Applied Geophysics* **162**, 461–477.
- Julivert M., Fontboté J.M., Ribeiro A. and Nabais Conde L.E. 1972. *Mapa Tectónico de la Península Ibérica y Baleares E. 1:1000000*. IGME Memoria explicativa.
- Lan H.X., Hu R.L., Yue Z.Q., Lee C.F. and Wang S.J. 2003. Engineering and geological characteristics of granite weathering profiles in South China. *Journal of Asian Earth Science* **21**, 353–364.
- Lee S.G. and de Freitas M.H. 1990. Seismic refraction surveys for predicting the intensity and depth of weathering and fracturing in granitic masses. In: *Field Testing in Engineering Geology* (eds E.G. Bell, M.G. Culshaw, J.C. Cripps and J.R. Coffey), pp. 241–256. Geological Society of London.
- Lotze W. 1945. Zur Gliederung der Varisziden der Iberischen Meseta. *Geotektonische Forsch* **6**, 78–92.
- Martin-Izard A., Paniagua A., García-Iglesias J., Fuertes M., Bixet L., Maldonado C. and Varela A. 2000. The Carlés copper-gold-molybdenum skarn (Asturias, Spain): Geometry, mineral associations and metasomatic evolution. *Journal of Chemical Exploration* **71**, 153–175.
- Miller R.D., Xia J., Park C.B. and Ivanov J.M. 1999. Multichannel analysis of surface waves to map bedrock. *The Leading Edge* **18**, 1392–1396.
- Park C.B., Miller R.D. and Xia J. 1998. Imaging dispersion curves of surface waves on multi-channel record. 68<sup>th</sup> SEG meeting, New Orleans, Louisiana, USA, Expanded Abstracts, 1377–1380.
- Park C.B., Miller R.D. and Xia J. 1999. Multichannel analysis of surface waves MASW. *Geophysics* **64**, 800–808.
- Popovici A.M. and Sethian J. 1997. Three dimensional traveltimes computation using the fast marching method. 67<sup>th</sup> SEG meeting, Dallas, Texas, USA, Expanded Abstracts, 1778–1781.
- Pullammanappallil S.K. and Louie J.N. 1994. A generalized simulated-annealing optimization for inversion of first-arrival times. *Bulletin of the Seismological Society of America* **84**, 1397–1409.
- Solé J., Arcos D., Soler A. and Delgado J. 1995. Datación K/Ar de las distintas mineralizaciones relacionadas con el stock granodiorítico de Carlés (Asturias). *Boletín de la Sociedad Española de Mineralogía* **18**, 31–32.
- Tardy Y. 1971. Characterization of the principal weathering types by the geochemistry of waters from some European and African crystalline massif. *Chemical Geology* **7**, 253–271.
- Xia J., Miller R.D. and Park C.B. 1999. Estimation of near-surface shear-wave velocity by inversion of Rayleigh waves. *Geophysics* **64**, 691–700.